Polyhedron 47 (2012) 151–164

Contents lists available at SciVerse ScienceDirect

Polyhedron

journal homepage: www.elsevier.com/locate/poly

Synthesis, structural, and biological evaluation of the arene-linked pyrazolyl methane ligands and their d^9/d^{10} metal complexes

Xin-Yu Wang [a], Shu-Qing Liu [b], Chun-Yan Zhang [b], Ge Song [a], Feng-Ying Bai [c,*], Yong-Heng Xing [a,*], Zhan Shi [d]

[a] College of Chemistry and Chemical Engineering, Liaoning Normal University, Dalian 11602, PR China
[b] College of Life Science, Dalian Medical University, Dalian 11602, PR China
[c] College of Life Science, Liaoning Normal University, Dalian 11602, PR China
[d] State Key Laboratory of Inorganic Synthesis and Preparative Chemistry, College of Chemistry, Jilin University, Changchun 130012, PR China

ARTICLE INFO

Article history:
Received 16 May 2012
Accepted 6 August 2012
Available online 18 August 2012

Keywords:
Arene-linked pyrazolyl methane ligands
Transition metal complexes
Cytotoxic activity
Crystal structure
Spectra properties

ABSTRACT

A series of the p-bis[(1-pyrazolyl)methyl] benzene ligands ($\mathbf{L_1}$–$\mathbf{L_6}$) in the DMSO system were synthesized. In the mean time, by using the ligands as a linker, a new family of transition metal coordination polymers, namely, $[Cu_2(\mathbf{L_1})_2Cl_4]$ (**1**), $[Cu_2(\mathbf{L_2})_2Cl_4]$ (**2**), $[Ag(\mathbf{L_2})(NO_3)]$ (**3**), $[Zn_2(\mathbf{L_2})_2(SCN)_4]$ (**4**) and $[Cd_2(\mathbf{L_2})(SCN)_4]$ (**5**) [$\mathbf{L_1}$ = 1,4-bis((1*H*-pyrazol-1-yl)methyl)benzene; $\mathbf{L_2}$ = 1,4-bis(3,5-dimethyl-1*H*-pyrazol-1-yl)methyl)benzene] have been constructed by the reaction of the p-bis[(1-pyrazolyl)methyl]benzene and corresponding to the transition metal compounds in a mixed solution of CH_3OH/C_2H_5OH at mild temperature condition. All the coordination polymers and p-bis[(1-pyrazolyl)methyl]benzene ligands were characterized by elemental analysis, IR spectroscopy, ^1H NMR and ^{13}C NMR, and some of them were characterized by UV spectroscopy, thermogravimetric analysis, X-ray powder and X-ray single-crystal diffraction. Structural analyses reveal that the ligands $\mathbf{L_3}$–$\mathbf{L_5}$ ($\mathbf{L_3}$ = 1,4-bis((4-iodo-1*H*-pyrazol-1-yl)methyl)benzene, $\mathbf{L_4}$ = 1,4-bis((4-iodo-3,5-dimethyl-1*H*-pyrazol-1-yl)methyl)benzene, $\mathbf{L_5}$ = 1,4-bis((4-nitro-1*H*-pyrazol-1-yl)methyl) benzene,$\mathbf{L_6}$ = 1,4-bis((4-nitro-3,5-dimethyl-1*H*-pyrazol-1-yl) methyl) benzene) are discrete organic compound molecules and the complexes **1**–**5** are 1D M–L–M coordination polymers, which are further interlinked via hydrogen bonds resulting in 2D or even 3D supermolecular networks. The luminescent properties of the coordination polymers **3**, **4** and **5** were examined by luminescence spectra. The analytic results indicate that different metal complexes with the same ligand have different influence on the characteristic photoluminescence. Furthermore, the cytotoxicity of the ligands $\mathbf{L_1}$–$\mathbf{L_6}$ and complexes **1**–**5** were evaluated against hepG2 cells. For the ligands of $\mathbf{L_1}$–$\mathbf{L_6}$, the different substituents of the pyrazole ring slightly influenced the cytotoxicity of the cell. It is found that nitro-compounds have shown the highest cytotoxicity under the same concentration condition. The cytotoxic activity of the complexes **1**–**5** are strongly increased by the introduction of the transition metals.

1. Introduction

Nowadays, as one of an attractive area of metal-organic frameworks, supramolecular coordination complexes have been prevalently investigated. A great deal of works have been made to design, synthesize and characteristic functional supramolecular complexes, because they exhibit promising application in wide fields of structural diversity, electronic properties [1,2], crystal engineering, supramolecular chemistry, biological activity [3,4], catalysis, sensors, pharmaceutical chemistry, etc. [5]. Apparently, the judicious choices of special inorganic and organic building blocks are the key steps for designing such materials with desired structural motifs and properties. Among the organic building blocks, N-heterocyclic ligands have been widely employed for this purpose. In particular, tris(pyrazolyl)borate (Tp) and tris(3,5-dimethylpyrazolyl) borate (Tp^*) are the simplest and most frequently encountered members of the scorpionate family, which were first developed by Trofimenko in the mid-1960s [6]. The ligand is named commonly as "the first generation" scorpionate ligand and possess an extremely versatile class of facially coordinating N-donors due to their ease of steric and electronic modification [7]. Therefore, they are investigated widely in a number of different purposes, including enzyme modelling, bioinorganic chemistry [8], polymerization catalysts [9] and SOD mimetics [10]. On the other hand, since synthesizing a series of "the second generation" scorpionate-like ligands of poly(pyrazolyl)-alkanes, which have prevalent polydentate nitrogen donor ligands [11], some researchers have contrasted the chemistry of complexes of the neutral

* Corresponding authors.
E-mail addresses: baifengying@yahoo.com.cn (F.-Y. Bai), xingyongheng2000@163.com (Y.-H. Xing).

0277-5387/$ - see front matter © 2012 Elsevier Ltd. All rights reserved.
http://dx.doi.org/10.1016/j.poly.2012.08.016

poly(pyrazolyl)alkanes with that of previously poly(pyrazolyl)borates. Similarly, although these ligands could also form a variety of coordination complexes with main groups and transition metal [12], complexes with poly(pyrazolyl)alkanes remain less to be investigated so far, because of great difficulties encountered in the process of preparing large amounts of these N-donor species. More recently, "the third generation" arene-linked a variety of nitrogen-based ligands, including pyrazolyl-pyrimidine, pyrazolyl-pyridazine and pyridyl-pyridazine [13,14], were successfully synthesized and employed [15], which are specifically functionalized at the non-coordinating "back" position to have an insight into the substances with uncommon solid state supramolecular architectures [16].

In order to further study the key roles in directing the final supramolecular structure, we start to extend our work by choosing special linear arene-linked p-bis[(1-pyrazolyl)methyl]benzene ligands (L_p), because the third-generation have not only rigid backbones but also flexible bis(pyrazolyl)methane units. Usually, the multiple coordination sites of the ligands can form the structures of higher dimensions and high symmetry. However, it is found that examples of high-dimensional supramolecular structures (2D and 3D) based on L_p ligand are rare up to now [17]. This phenomenon could be attributed to the linear geometry of the ligand where donor groups are linked by a rigid spacer and the chelating coordination mode adopted by the bis(pyrazolyl)methane units.

Recently, a series of benzene-linked mono-, bis(pyrazolyl)methane units (the third-generation) were synthesized by introducing different substituents into the pyrazole ring. Due to the inherent chemistry characteristic of benzene-linker, they present many virtues as follows: mono-, bis(pyrazolyl) methane units directly fused to an benzene ring to result in the formation of binuclear metallacyclic complexes, making the structures of the complexes with higher symmetry [18]; Moreover, pyrazolyl groups can freely twist around alkyl groups with different angles to generate different conformations and coordination modes, and form a variety of supramolecular coordination complexes; Additionally, it is found that they have an effective biological activity about inhibiting cancer cell growth [19].

To our best knowledge, the complexes of benzene-linker reported by predecessors were mainly classified into three types as follows: (i) benzene-linked di-pyrazolyl complexes of Cu(II), Cd(II), Co(II) [20,21]; (ii) benzene-linked tetra-pyrazolyl complexes of Ag(I), Ni(II), Co(II), Ir(II), Rh(II), Zn(II)and Fe(I) [16,22,23]; (iii) benzene-linked hexa-pyrazolyl complexes of Zn(II) and Re(I) [16,24]. The most works were focused on type (ii), however, benzene-linked dipyrazolyl ligands are rarely used to prepare metal–organic complexes with interesting structures, functional properties, especially the luminescent property of the complexes. In this paper, our group used 1,4-bis(bromomethyl)benzene and pyrazole/its derivatives as raw materials, a series of benzene ring-linked pyrazolyl methane ligands (**L_1–L_6**) in the DMSO system were synthesized [25]. In particular, based on this linear ligands [1,4-bis((1*H*-pyrazol-1-yl)methyl)benzene(L1);1,4-bis((3,5-dimethyl-1*H*-pyrazol-1-yl)methyl)benzene(L2)], corresponding to the complexes were designed and synthesized firstly by regulating proper reaction conditions. Fortunately, we obtained and characterized a series of the novel copper(II), silver(I), zinc(II) and cadmium(II) complexes. In addition, we have tested the biological activity of the ligands **L_1–L_6** and complexes **1**–**5**, with the purpose of comparing the variation in biological activity of the changing different substituted groups for ligands and different metal complexes. In general, the aim of this report is to give a detailed synthesis rule and further systematic investigation on bioactivity of the ligands and corresponding complexes.

2. Experimental

2.1. Materials and general procedure

All chemicals purchased were of reagent grade or better and were used without further purification. Biological reagent: Dulbecco's modified Eagle's medium (DMEM) was purchased from Hycone and fetal bovine serum (FBS) was purchased from TBD (Tian Jin, China). The trypsin was purchased from Gibco Invitrogen Corporation (Grand Island, NY, USA). Dimethyl sulfoxide (DMSO), 3(4,5-dimethylthiazole-2-yl)-2,5-diphenyltetrazolium (MTT) were purchased from Sigma (St. Louis MO, USA). DMSO in cells was maintained at 0.5%, which had no effect on cell growth or apoptosis. The infrared spectra were recorded on a JASCO FT/IR-480 PLUS Fourier Transform spectrometer with pressed KBr pellets in the range 200–4000 cm^{-1}. The elemental analyses for C, H, and N were carried out on a Perkin Elmer 240C automatic analyzer. The luminescence spectra was reported on a JASCO F-6500 spectrofluorimeter (solid). UV–Vis absorption spectra diffuse reflection was recorded with a UV–Vis/NIR spectrophotometer of JASCO V–570 in the 200–2500 nm (solid sample). Thermogravimetric analyses (TGA) were performed under N_2 atmosphere at 1 aim with a heating rate of 10 °C/min on a Perkin Elmer Diamond TG/DTA. The ^1H and ^{13}C spectra were recorded on BrukerAV-500 apparatus ($CDCl_3$ or DMSO-d_6 as solvent, TMS internal standard). X-ray powder diffraction (PXRD) patterns were obtained on a Bruker Advance-D8 equipped with CuKa radiation, in the range $5° < 2\theta < 60°$, with a step size of 0.02° (2θ) and an count time of 2 s per step.

2.2. Synthesis

2.2.1. Synthesis of the ligands

2.2.1.1. Precursor: 1,4-bis(bromomethyl)benzene. It was prepared as a method previously described [27]. Briefly, 29.6 mL (0.24 mol) dry p-xylene was introduced into the flask, stirring at 140 °C in an oil bath. When the xylene starts boiling, 24.6 mL (0.48 mol) of dry bromine were added dropwise over 2 h and using a 300-watt tungsten lamp lighted reaction. To continued at 140 °C for an additional 3 h. Then, the mixture is cooled over night and dissolved in resultant of warm chloroform. And the precipitate was dissolved in fresh chloroform solution and recrystallizing in it. Yield: 55.4 g (87.4%). m.p.:143–146 °C. *Anal.* Calc. for $C_8H_8Br_2$: C, 36.40; H, 3.05. Found: C, 36.29; H, 3.37%. FT-IR (KBr, cm^{-1}): 3050, 3036(=C–H); 2972 (C–H); 1512, 1437(C_{ph}–C_{ph}; C_{ph}=C_{ph}); 611(C–Br). ^1H NMR (500 MHz, DMSO-d_6, δ/ppm): 7.43 (s, 4H, ph), 4.69 (s, 4H, –CH_2).

Ligands (**L_1–L_6**) were prepared according to the similar or modified references [26,28,29]. A mixed solution of pyrazole (1.02 g, 15 mmol) **(L_1)** or its derivates (3,5-dimethyl-1*H*-pyrazole (1.47 g, 15 mmol) **(L_2)**, 4-iodo-1*H*-pyrazol (2.19 g, 15 mmol) **(L_3)**, 4-iodo-3,5-dimethyl-1*H*-pyrazole (3.33 g, 15 mmol) **(L_4)**, 4-nitro-1*H*-pyrazole (1.70 g, 15 mmol) **(L_5)**, 4-nitro-3,5-dimethyl-1*H*-pyrazol (2.12 g, 15 mmol) **(L_6)**) and 82% potassium hydroxide (1.02 g, 15 mmol) in DMSO (10 mL) were vigorously stirred at 80 °C for 1 h. Then, 1,4-bis(bromomethyl)benzene (1.98 g, 7.5 mmol) in DMSO (15 mL) was added dropwise to the solution above over 30 min, keeping the reaction at 80 °C to continue stirring for 5–10 h. The mixture was poured into 200 mL of H_2O and an amount of precipitates occurred. Finally, the precipitate was filtered and dried in the air. The precipitate was dissolved in the fresh chloroform solution and re-crystallized from it. The characterization data of the ligands **L_1–L_6** were listed in Table 1 and the detailed appointments of the IR spectra data are given in Table S1.

2.2.2. Synthesis of the complexes

The complexes **1**–**5** were prepared by the mixed solution reaction of EtOH and MeOH. The starting material ($CuCl_2{\cdot}2H_2O$

Table 1
The characterization data of the ligands $\mathbf{L_1}$–$\mathbf{L_6}$.

Compounds	Elemental analyses (%)	^{1}H NMR, δ, ppm	^{13}CNMR, δ, ppm	Yield, m.p.
$\mathbf{L_1}$	Calc. for $C_{14}H_{14}N_4$: C, 70.57; H, 5.92; N, 23.51. Found: C, 70.49; H, 5.88; N, 23.63%	7.53 (d, 2H, H^5-pz, J = 1.7 Hz), 7.36 (d, 2H, H^3-pz, J = 2.2 Hz), 7.17 (s, 4H, ph), 6.27 (t, 2H, H^4-pz, $J_1 = J_2$ = 2.1 Hz), 5.30 (s, 4H, CH_2)	139.62, 136.55, 129.24, 128.04, 106.02, 55.52	1.23 g (68.9%) 111.5–1121 °C
$\mathbf{L_2}$	Calc. for $C_{18}H_{22}N_4$: C, 73.44; H, 7.53; N, 19.03. Found: C, 73.57; H, 7.32; N, 19.11%	7.00 (s, 4H, ph), 5.82 (s, 2H, H^4-pz), 5.16 (s, 4H, CH_2), 2.22 (s, 6H, 5-CH_3-pz), 2.12 (s, 6H, 3-CH_3-pz)	147.58, 139.11, 136.68, 126.92, 105.54, 52.23, 13.48, 11.07	1.35 g (61.2%) 101–102 °C
$\mathbf{L_3}$	Calc. for $C_{14}H_{12}N_4I_2$: C, 34.31; H, 2.47; N, 11.43. Found: C, 34.23; H, 2.55; N, 11.38%	7.53 (s, 2H, H^5-pz), 7.40 (s, 2H, H^3-pz), 7.20 (s, 4H, ph), 5.28 (s, 4H, CH_2)	144.76, 136.10, 133.67, 128.37, 56.62, 56.01	2.81 g (76.5%) 157–158 °C
$\mathbf{L_4}$	Calc. for $C_{18}H_{20}N_4I_2$: C, 39.58; H, 3.69; N, 10.26. Found: C, 39.46; H, 3.55; N, 10.31%	7.02 (s, 4H, ph), 5.23 (s, 4H, CH_2), 2.23 (s, 6H, 5-CH_3-pz); 2.16 (s, 6H, 3-CH_3-pz)	149.55, 140.68, 136.29, 127.16, 63.27, 53.59, 14.04, 12.04	3.62 g (88.4%) 188–191 °C
$\mathbf{L_5}$	Calc. for $C_{14}H_{12}N_6O_4$: C, 51.22; H, 3.68; N, 25.60. Found: C, 51.18; H, 3.59; N, 25.68%	9.02 (s, 2H, H^5-pz), 8.25(s, 2H, H^3-pz), 7.34 (s, 4H, ph), 5.39 (s, 4H, CH_2)	135.91, 135.68, 135.04, 130.58, 128.36, 55.37	1.61 g (65.4%). 269.9–271 °C
$\mathbf{L_6}$	Calc. for $C_{18}H_{20}N_6O_4$: C, 56.24; H, 5.24; N, 21.86. Found: C,56.18; H, 5.17; N, 21.94%	7.13 (s, 4H, ph), 5.24 (s, 4H, CH_2), 2.55 (s, 6H, 5-CH_3-pz), 2.52 (s, 6H, 3-CH_3-pz)	146.38, 140.29, 135.26, 127.67, 53.20, 14.14, 11.69	1.78 g (61.8%), 188.5–189.4 °C

(0.0170 g, 0.1 mmol) for complexes **1** and **2**, $AgNO_3$ (0.0170 g, 0.1 mmol) for **3**, $ZnSO_4{\cdot}7H_2O$ (0.0287 g, 0.1 mmol) for **4**, $Cd(NO_3)_2{\cdot}4H_2O$ (0.0308 g, 0.1 mmol) for **5**) and corresponding to ligands ($\mathbf{L_1}$ (0.0238 g, 0.1 mmol) for **1**, $\mathbf{L_2}$ (0.0294 g, 0.1 mmol) for **2**–**5**) in CH_3OH (15 mL) were dissolved in a 50 mL of the conical flask. After a solution of oxalic acid (0.045 g, 0.5 mmol) for **1**, KSCN (0.0292 g, 0.3 mmol) for **4** or **5** dissolved in methanol of 5 mL was added dropwise to it, a precipitate is formed immediately, then the solution was refluxed for 3 h and filtered, the precipitate was washed with methanol and then dried at room temperature. Corresponding crystals of the complexes (**1**–**5**) suitable for X-ray diffraction analysis crystallized from mother liquid. The characterization data and the detailed appointment of the IR spectra data for complexes **1**–**5** were listed in Table 2 and S2, respectively.

2.3. Cell line and culture

HepG-2 cell line derived from a human hepatocellular carcinoma was given by Peking Union Medical College. Cells were cultured in DMEM medium supplemented with 10% FBS, 100 U mL^{-1} penicillin and l00 μg mL^{-1} streptomycin, being maintained at 37 °C with 5% CO_2 in a humidified atmosphere.

2.4. Cell viability assay

The viability of the cells was assessed by MTT assay [30]. To be specific, cells were detached and seeded in a 96-well plate (5×10^4 cells/well) and after 12 h, the medium was exchanged. Compounds in different concentrations were incubated for a period of 24 h, during this period, 20 μL of 1-(4,5-dimethylthiazol-2-yl)-3,5-diphenylformazan (MTT) solution (5.0 mg mL^{-1} in PBS) were added to each well, which was incubated for an additional 4 h. Subsequently, the medium was removed carefully, and 150 μL of DMSO was added. Cell viability was determined by absorbance measurements at 490 nm. In fact, the absorbance we measured is correlated to a new produced blue compound, which was named formazan. Calculate the rate of cell viability: Rate of cell growth inhibition = AT/AC × 100%. AC was the absorbance for control set, the same concentration of DMSO solvent with empty synthetic compounds; AT was treated with series of compounds at individual concentration.

2.5. X-ray crystallographic determination

Suitable single crystals of three compounds and five complexes were mounted on glass fibers for X-ray measurement, respectively. Reflection data were collected at room temperature on Rigaku R-

Table 2
The characterization data of complexes **1**–**5**.

Complexes	Molecular formula	Elemental analyses (%)	Yield
1	$C_{28}H_{28}N_8Cu_2Cl_4$	Calc.: C, 46.11; H, 3.79; N, 15.03. Found: C, 45.02; H, 3.69; N, 14.98%	0.0315 g (77.40%)
2	$C_{36}H_{44}N_8Cu_4Cl_4$	Calc.: C, 50.41; H, 5.17; N, 13.06; Found: C, 50.10; H, 5.15; N,13.02%	0.0329 g (76.69%)
3	$C_{18}H_{22}N_5O_3Ag$	Calc.: C, 46.57; H, 4.78; N, 15.08. Found: C, 46.49; H, 4.75; N, 15.02.	0.0309 g (66.60%)
4	$C_{40}H_{44}N_{12}S_4Zn_2$	Calc.: C, 52.22; H, 5.58; N, 16.61. Found: C, 55.18; H: 5.54; N, 16.59%	0.0358 g (75.21%)
5	$C_{22}H_{22}N_8Cd_2S_4$	Calc.: C, 35.16; H, 2.95; N, 14.91. Found: C, 35.11; H, 2.92; N, 14.89%	0.0498 g (66.26%)

Table 3
Crystallographic data for the compounds $\mathbf{L_3}$, $\mathbf{L_4}$ and $\mathbf{L_5}$.[a]

Compounds	$\mathbf{L_3}$	$\mathbf{L_4}$	$\mathbf{L_5}$
Formula	$C_7H_6N_2I$	$C_9H_{10}N_2I$	$C_7H_6N_3O_2$
Mr (g mol^{-1})	245.04	273.09	164.15
Crystal system	triclinic	monoclinic	monoclinic
Space group	$P\bar{1}$	$P2_1/c$	$P2_1/c$
a (Å)	4.5306(10)	7.5347(11)	11.151(2)
b (Å)	8.2058(18)	14.945(2)	4.5954(9)
c (Å)	11.009(2)	8.7180(12)	14.707(3)
α (°)	73.492(2)	90	90
β (°)	82.107(3)	95.782(2)	106.20(3)
γ (°)	75.042(3)	90	90
V (Å^3)	378.22(14)	976.7(2)	723.7(2)
Z	2	4	4
D_{calc} (g cm^{-3})	2.152	1.857	1.507
Crystal size (mm)	0.67 × 0.19 × 0.17	0.31 × 0.22 × 0.11	0.21 × 0.16 × 0.05
F(000)	230	524	340
μ (MoKα) (mm^{-1})	4.153	3.227	0.115
θ (°)	2.66–25.00	2.72–25.00	3.18–27.45
Reflections collected	1875	4795	6409
Independent reflections ($I > 2\sigma(I)$)	1299(1224)	1706(1527)	1641(961)
Parameters	91	111	109
Δ (ρ) (e Å^{-3})	0.844, −1.384	0.425, −1.879	0.156, −0.221
Goodness-of-fit (GOF)	1.266	1.210	1.053
R[a]	0.0342(0.0359)[b]	0.0412(0.0449)[b]	0.0582(0.1053)[b]
wR_2[a]	0.1060(0.1071)[b]	0.1043(0.1069)[b]	0.1198(0.1371)[b]

[a] $R = \Sigma||F_o|-|F_c||/\Sigma|F_o|$, $wR_2 = \{\Sigma[w(F_o^2-F_c^2)^2]/\Sigma[w(F_o^2)^2]\}^{1/2}$; $[F_o > 4\sigma(F_o)]$.
[b] Based on all data.

AXIS RAPID IP (compounds $\mathbf{L_3}$ and $\mathbf{L_4}$, complex **1**) and Bruker SMART APEX II CCD ($\mathbf{L_5}$ and complexes **2**–**5**) diffractometer with graphite monochromatized MoKα radiation (λ = 0.71073 Å). All absorption corrections were performed using the SADABS program [31]. Crystal structures were solved by the direct method. All non-hydrogen atoms were refined anisotropically. Hydrogen atoms of ligands were fixed at calculated positions with isotropic thermal parameters. All calculations were performed using the SHELX-97 program [32]. Crystal data and details of the data collection and the structure refinements of ligands $\mathbf{L_3}$–$\mathbf{L_5}$ are given in Table 3 and those of the complexes **1**–**5** are given in Table 4. The selected bond lengths and bond angles of the ligands $\mathbf{L_3}$–$\mathbf{L_5}$ and the complexes **1**–**5** are listed in Table 5. The drawings for all compounds and complexes were made with Diamond 3.2.

3. Results and discussion

3.1. Synthesis

By doing a great deal of experiment, it is found that it is especially crucial to meet the higher yield and quality of both looking for suitable pyrazole/its derivatives as a raw material and regulating proper reaction conditions. For this purpose, we designed and synthesized different types of pyrazolyl derivatives with iodination or nitration substituted groups at first (shown in the Scheme 1). Then by the reaction of pyrazole/its derivatives with 1,4-bis(bromomethyl)benzene in the DMSO system, furthermore, we obtained a series of $\mathbf{L_1}$–$\mathbf{L_6}$ ligands (shown in the Scheme 2). During the reaction above, it is found that the reaction result is affected by the factors of steric obstacle, substitution groups and reaction conditions. In particular, the influence of the steric obstacle of the substituted groups on pyrazolyl derivatives is the most important. So, the reaction of 3,5-dimethylpyrazole/its derivatives with 1,4-bis(bromomethyl)benzene were more difficult than those of pyrazole/its derivatives(4-I/NO_2 substituted on pyrazolyl ring).

To get higher yields of the target products, it is found that the optimization reaction condition of 1,4-bis(bromomethyl)benzene with pyrazole/its derivatives is at a molar ratio of 1:2 and starting reaction material of 1,4-bis(bromomethyl)benzene should be added dropwise.

By the solvent reaction method, complexes **1**–**5** have been successfully generated at the first time (Scheme 3). The crystalline solids are all soluble in most polar solvent. Here we have done our best to search for the optimistic reaction conditions for improving

Table 4
Crystallographic data for complexes **1-5**.[a]

Complexes	**1**	**2**	**3**	**4**	**5**
Formula	$C_{14}H_{14}N_4Cl_2Cu$	$C_9H_{11}N_2ClCu_{0.5}$	$C_9H_{11}N_{2.5}O_{1.5}Ag_{0.5}$	$C_{20}H_{22}N_6S_2Zn$	$C_{11}H_{11}N_4S_2Cd$
Mr (g mol^{-1})	372.73	214.42	232.14	475.93	375.79
Crystal system	monoclinic	monoclinic	monoclinic	triclinic	triclinic
Space group	$P2_1/n$	$C2/c$	$C2/c$	$P\bar{1}$	$P\bar{1}$
a (Å)	8.8153(12)	14.723(3)	11.340(2)	10.038(2)	8.9615(18)
b (Å)	12.9316(18)	8.4311(17)	14.189(3)	11.057(2)	9.0061(18)
c (Å)	13.1313(18)	17.514(4)	12.358(3)	11.445(2)	9.1711(18)
α (°)	90	90	90	71.81(3)	85.29(3)
β (°)	92.685(2)	114.14(3)	102.17(3)	74.48(3)	76.67(3)
γ (°)	90	90	90	86.08(3)	76.05(3)
V (Å^3)	1495.3(4)	1983.9(7)	1943.8(7)	1162.7(4)	698.7(2)
Z	4	8	8	2	2
D_{calc} (g cm^{-3})	1.656	1.436	1.587	1.359	1.786
Crystal size (mm)	0.43 × 0.09x0.08	0.37 × 0.25 × 0.13	029 × 0.16 × 0.08	029 × 0.16 × 0.07	032 × 0.25 × 0.13
F(000)	756	884	944	492	370
μ (MoKα) (mm^{-1})	1.815	1.378	1.065	1.253	1.848
θ (Å^3)	2.21–24.99	3.03–27.49	3.10–24.99	3.13–27.48	3.22–27.48
Reflections collected	7357	9429	7415	10768	6897
Independent reflections ($I > 2\sigma(I)$)	2632	2264	1710	5050	3178
Parameters	190	117	124	262	174
Δ (ρ) (e Å^{-3})	0.294, −0.292	0.401, −0.341	2.667, −0.977	1.621, −0.976	0.567, −0.609
Goodness of fit	1.067	1.027	1.120	1.107	1.244
R[a]	0.0328 (0.0483)[b]	0.0369 (0.0496)[b]	0.0807 (0.0875)[b]	0.1169 (0.1468)[b]	0.0256 (0.0288)[b]
wR_2[a]	0.0749 (0.0804)[b]	0.0822 (0.0894)[b]	0.2773 (0.2828)[b]	0.3395 (0.3552)[b]	0.0845 (0.0986)[b]

[a] $R = \Sigma||F_o|-|F_c||/\Sigma|F_o|$, $wR_2 = \{\Sigma[w(F_o^2-F_c^2)^2]/\Sigma[w(F_o^2)^2]\}^{1/2}$; $[F_o > 4\sigma(F_o)]$.
[b] Based on all data.

Table 5
Selected bond distances (Å) and angles (°) of the compounds and complexes.*

L_3					
I(1)–C(2)	2.066(6)	C(1)–N(1)	1.343(8)	C(1)–C(2)	1.383(8)
C(2)–C(3)	1.379(8)	C(3)–N(2)	1.328(8)	C(4)–N(1)	1.458(8)
C(4)–C(5)	1.503(8)	C(5)–C(6)	1.387(8)	C(6)–C(7)	1.381(8)
N(1)–N(2)	1.360(7)	C(5)–C(7)$^{\#1}$	1.393(8)	C(7)–C(5)$^{\#1}$	1.393(8)
N(1)–C(4)–C(5)	111.4(5)	C(3)–C(2)–I(1)	128.6(4)	C(1)–C(2)–I(1)	126.4(4)
L_4					
C(3)–I(1)	2.073(5)	C(2)–N(1)	1.349(6)	C(1)–C(2)	1.501(6)
C(2)–C(3)	1.369(7)	C(3)–C(4)	1.403(7)	C(4)–N(2)	1.337(7)
C(4)–C(5)	1.491(7)	C(6)–N(1)	1.447(5)	C(6)–C(7)	1.525(6)
C(7)–C(9)	1.379(6)	C(7)–C(8)	1.381(6)	C(8)–C(9)$^{\#1}$	1.384(7)
C(9)–C(8)$^{\#1}$	1.385(7)	N(1)–N(2)	1.362(5)	N(1)–C(6)–C(7)	114.1(4)
C(2)–C(3)–I(1)	124.7(3)	C(4)–C(3)–I(1)	128.3(4)		
L_5					
N(3)–O(1)	1.221(2)	N(3)–O(2)	1.223(3)	C(1)–C(2)	1.380(3)
C(1)–C(3)$^{\#1}$	1.383(3)	C(2)–C(3)	1.382(3)	C(2)–C(4)	1.509(3)
C(4)–N(1)	1.469(3)	C(5)–N(2)	1.321(3)	C(5)–C(6)	1.384(3)
C(6)–C(7)	1.373(3)	C(6)–N(3)	1.417(3)	N(1)–N(2)	1.365(3)
N(1)–C(4)–C(2)	111.79(18)	O(1)–N(3)–O(2)	122.5(2)	O(1)–N(3)–C(6)	118.7(2)
Complex 1					
Cu–N(1)	2.002(2)	Cu–N(3)	2.011(2)	Cu–Cl(3)	2.2306(9)
Cu–Cl(2)	2.2528(9)				
N(1)–Cu–N(3)	153.41(9)	N(1)–Cu–Cl(3)	93.61(7)	N(3)–Cu–Cl(3)	98.71(7)
N(1)–Cu–Cl(2)	91.29(7)	N(3)–Cu–Cl(2)	89.27(7)	Cl(3)–Cu–Cl(2)	150.94(4)
Complex 2					
N(2)–Cu	1.977(2)	Cu–Cl(1)	2.2511(8)	N(1)–N(2)	1.364(3)
C(2)–N(2)	1.330(3)				
N(2)$^{\#2}$–Cu–N(2)	180.0	N(2)–Cu–Cl(1)$^{\#2}$	89.37(6)	N(2)–Cu–Cl(1)	90.63(6)
C(2)–N(2)–Cu	127.5(2)	N(1)–N(2)–Cu	126.4(2)		
Complex 3					
Ag–N(2)	2.210(8)	Ag–O(1)	2.59(1)	N(2)–N(3)	1.33(1)
C(4)–N(2)	1.34(1)				
N(2)$^{\#1}$–Ag–N(2)	129.9(4)	N(2)$^{\#1}$–Ag–O(1)$^{\#1}$	116.9(4)	N(2)–Ag–O(1)$^{\#1}$	108.8(4)
O(1)$^{\#1}$–Ag–O(1)	47.3(4)				
Complex 4					
Zn–N(2)	1.93(1)	Zn–N(1)	1.96(1)	Zn–N(4)	2.019(9)
Zn–N(5)	2.053(9)	N(3)–N(4)	1.37(1)	C(8)–N(4)	1.37(1)
N(2)–Zn–N(1)	109.9(5)	N(2)–Zn–N(4)	108.7(4)	N(1)–Zn–N(4)	110.4(4)
N(2)–Zn–N(5)	109.0(4)	N(1)–Zn–N(5)	104.3(4)	N(4)–Zn–N(5)	114.5(4)
Complex 5					
Cd–N(3)$^{\#1}$	2.270(4)	Cd–N(4)	2.295(3)	Cd–N(2)	2.297(3)
Cd–S(2)	2.609(1)	Cd–S(1)	2.735(1)	N(1)–N(2)	1.351(4)
C(2)–N(2)	1.341(4)				
N(3)$^{\#1}$–Cd–N(4)	90.9(2)	N(3)$^{\#1}$–Cd–N(2)	107.9(1)	N(4)–Cd–N(2)	88.4(1)
N(3)$^{\#1}$–Cd–S(2)	102.5(1)	N(4)–Cd–S(2)	92.8(1)	N(2)–Cd–S(2)	149.52(8)
N(3)$^{\#1}$–Cd–S(1)	92.3(1)	N(4)–Cd–S(1)	176.0(1)	N(2)–Cd–S(1)	92.99(8)
S(2)–Cd–S(1)	84.18(4)				

* Symmetry transformations used to generate equivalent atoms: #1: −x+1, −y, −z for **L_3**; #1: −x+2, −y, −z for **L_5**; #2: −x+1/2, −y+1/2, −z+1 for **2**; #1: −x+1, y, −z+1/2 for **3**; #1: −x+2, −y, −z+1 for **5**.

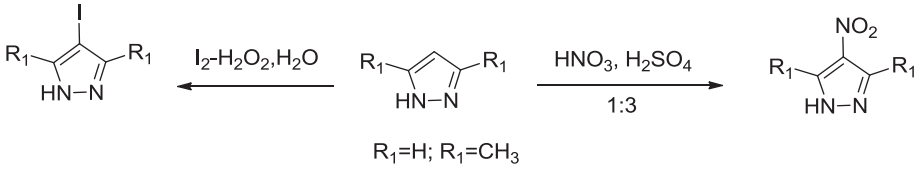

Scheme 1. The synthetic routes of 4-iodo-pyrazole and 4-nitro-pyrazole.

coordination ability of the ligands with metal atoms. We designed a reaction of $CuCl_2{\cdot}2H_2O$ or $AgNO_3$ and **L_2** with molar ratio 1:1 and got successfully single crystals of the complexes **2** and **3**, respectively. However, in the same reaction system, we could not get fine single crystals of the complexes **4** and **5**. Then, the addition of KSCN (0.3 mmol) promoted the formation of the single crystals of the complexes **4** and **5**. The results show that some small molecular reagents are in the favor of the crystal growing of the complexes. In order to further study influence about coordination capability of the ligands, we attempted to change **L_2** into **L_1**, when the molar ratio of starting material ($CuCl_2{\cdot}2H_2O$) and **L_1** ligand is still 1:1, complex **1** was not observed in the absolute methanol system at ambient temperature. Later, by adding 5 equivalent aliphatic acid (0.5 mmol), such as oxalic acid, succinic acid, glutaric acid, etc.,

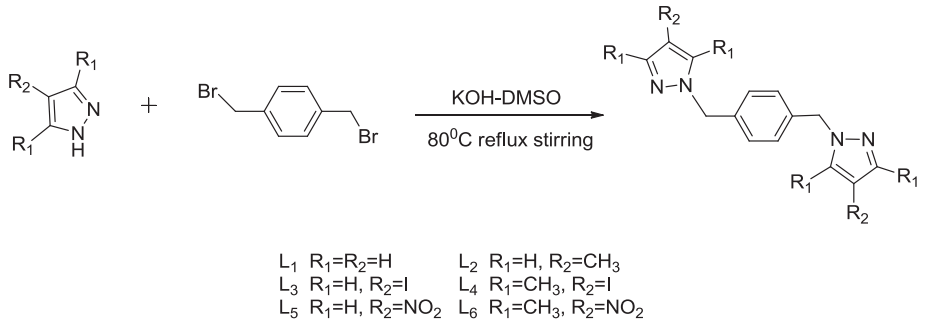

L_1 R_1=R_2=H L_2 R_1=H, R_2=CH_3
L_3 R_1=H, R_2=I L_4 R_1=CH_3, R_2=I
L_5 R_1=H, R_2=NO_2 L_6 R_1=CH_3, R_2=NO_2

Scheme 2. The synthetic routes of the ligands L_1–L_6.

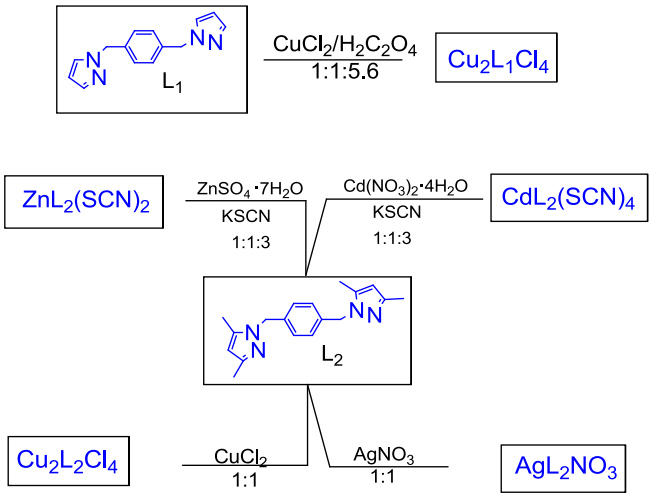

Scheme 3. The synthetic routes of the complexes **1–5**.

we obtained the objective complex **1**. Through these experiments, it is found that aliphatic acid in the reaction process may be as an important organic structural directing reagent, showing that the particular role of the molecular reagent in the reaction process may be a sensitive reaction parameter or participation co-ordination which seems to affect one of the factors for preparation of the complexes.

Table 6
Selected bond distances (Å) and angles (°) of the ligands L_3–L_5.

Compounds	L_3	L_4	L_5
C_{pz}–N_{pz}(av)	1.335(8)	1.343(7)	1.321(3)
C_{pz}–C_{pz}(av)	1.381(8)	1.386(7)	1.378(3)
N_{pz}–N_{pz}	1.360(7)	1.362(5)	1.365(3)
N_{pz}–C_{-CH2}	1.458(8)	1.447(5)	1.469(3)
C_{ph}–C_{-CH2}	1.503(8)	1.525(6)	1.509(3)
C_{ph}–C–N_{pz}	111.4(5)	114.1(4)	111.79(18)

3.2. Crystal structure analysis

3.2.1. Structural description of L_3–L_5

The asymmetric unit of the compounds L_3–L_5 is made up of a half molecule (Fig. 1a–c). In the structures of the compounds, all carbon atoms of the benzene ring form a good plane, the average of C–C distances and C–C–C angles from the ring are consistent with those reported in the literatures [33]. The dihedral angle between the benzene ring and the pyrazole ring is 76.5(3) for L_3, 84. 6(4) for L_4 and 74.7(2)° for L_5, respectively. In addition, there is a kind of hydrogen bond (C–H···O) in the molecule of L_5 between the carbon (donor) from benzene ring and oxygen (acceptor) from

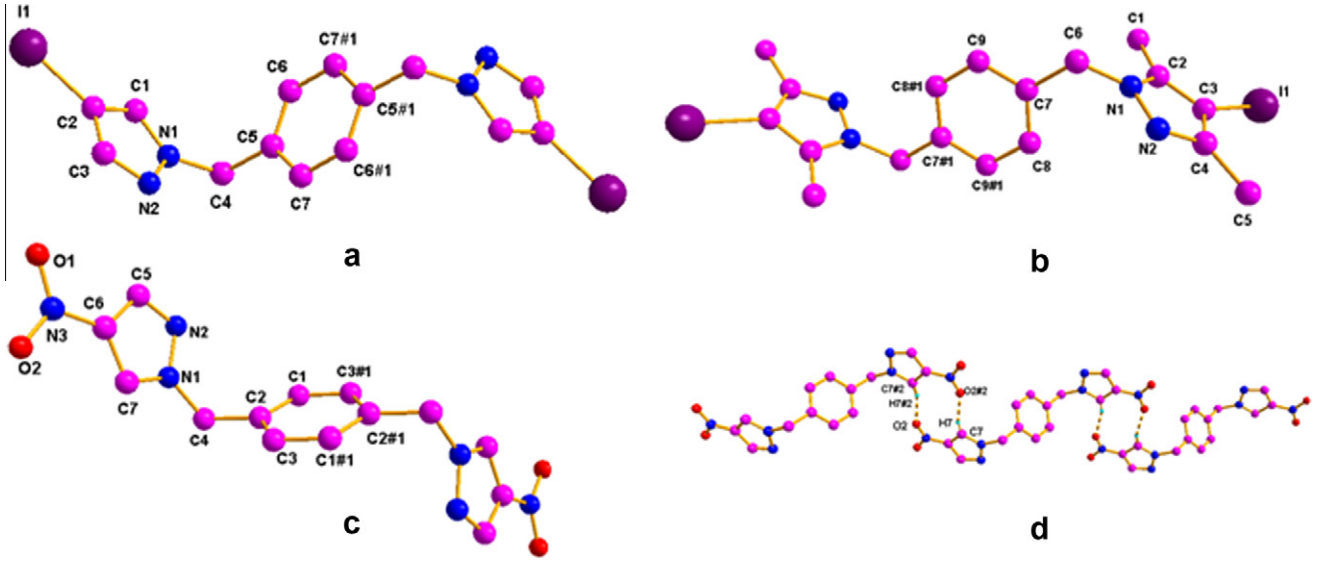

Fig. 1. (a) Molecular structure of the compounds (a) for L_3, (b) for L_4, (c) for L_5. (d) A view of a chain structure of L_5.(hydrogen atoms are omitted for clarity) (#1: −x+1, −y, −z for L_3; #1: −x+1, −y, −z+1 for L_4. #1: −x+2, −y, −z; #2: 1−x, 1−y, −z for L_5).

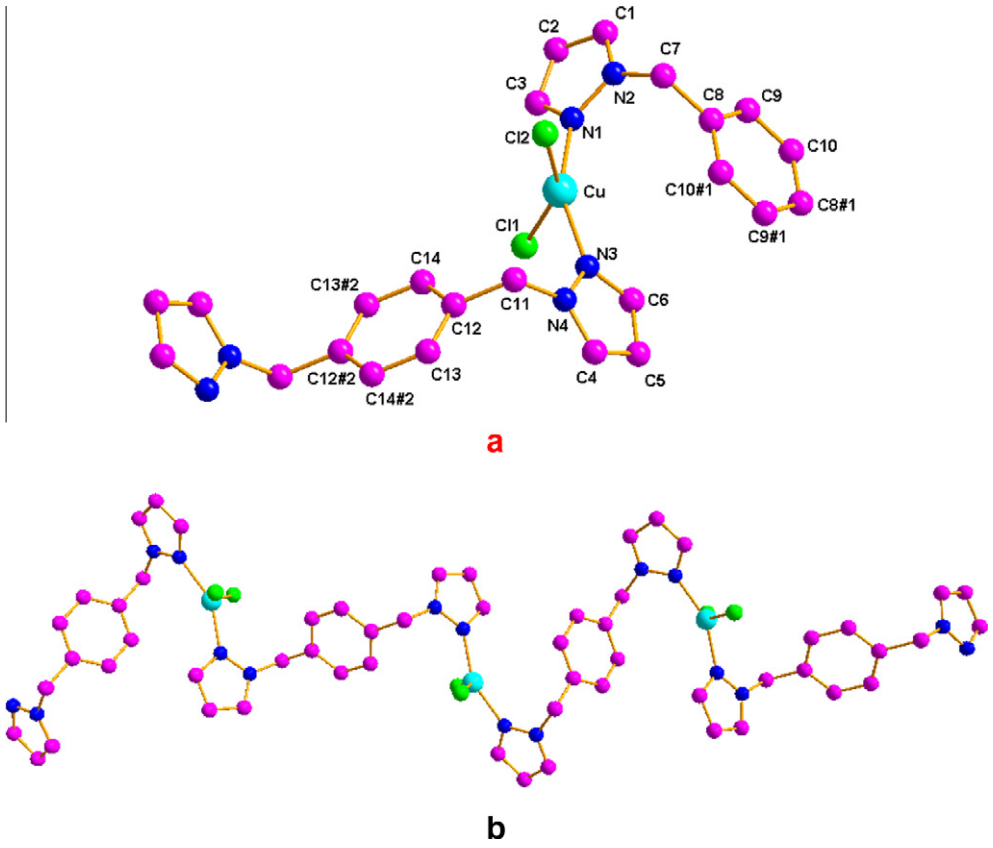

Fig. 2. (a) Local coordination environment of the Cu(II) atom in the complex **1**. (b) A view of a chain structure of the complex **1** (the hydrogen atoms are omitted for clarity) (#1: 2−x, −y, 2−z; #2: 2−x, 1−y, 1−z).

nitryl group. The molecules are connected by the hydrogen bond (C7–H7···O2$^{\#2}$, 3.2204 Å, 162.62°, #2: 1−x, 1−y,−z) forming an infinite chain(Fig. 1d). The C–I distances of $\mathbf{L_3}$ and $\mathbf{L_4}$ are 2.066(6) and 2.073(5) Å, respectively. As for $\mathbf{L_5}$, the bond length of C–N_{NO2} is 1.417(3) Å, the average distance of N–O bonds of nitryl group is 1.222(3) Å (N–O, 1.46 Å and N═O, 1.14 Å), O–N–O bond angle is 122.5(2)°.

The comparison of the corresponding bond lengths and bond angles of $\mathbf{L_3}$–$\mathbf{L_5}$ are listed in Table 6. The average bond distances of C_{pz}–C_{pz}, N_{pz}–N_{pz} and C_{pz}–N_{pz} from the pyrazole ring are similar to each other, showing that the different substitution groups (–NO_2, –I) from the pyrazole ring have little influence on the corresponding bond lengths of the compounds. In addition, it is found that the corresponding bond lengths and angles of N_{pz}–C–CH_2, C_{ph}–C–CH_2, C_{ph}–C–N_{pz} of $\mathbf{L_3}$ and $\mathbf{L_5}$ are also close each other, while that of $\mathbf{L_4}$ is slightly bigger than those of $\mathbf{L_3}$ and $\mathbf{L_5}$. It may be related to the steric factor of the substituents from the pyrazolyl ring.

3.2.2. Structural descriptions of 1–5

*3.2.2.1. $[Cu(\mathbf{L_1})Cl_2]_n$ (**1**).* X-ray single crystal diffraction analysis shows that the asymmetric unit contains one Cu(II) atom, one $\mathbf{L_1}$ ligand, and two Cl atoms (Fig. 2a). The Cu(II) atom displays a distorted tetrahedron geometry, and it is coordinated by two nitrogen atoms (N1, N3) from two $\mathbf{L_1}$ ligands and two chlorine atoms(Cl1, Cl2). $\mathbf{L_1}$ links two Cu^{2+} ions and adopts the bidentate coordination mode. The bond distances of Cu–N_{pz} and Cu–Cl are in the range of 2.002(2)–2.011(2) and 2.2306(9)–2.2528(9) Å, respectively, which is consistent with those in similar copper complexes [34]. The N–Cu–N bond angle is 153.41(9)°, the N–Cu–Cl angles are in the range of 89.27(7)–98.71(7)°. The dihedral angles between the pyrazole ring and the pyrazole ring/benzene ring are in the range of 68.8(2)–78.9(1)°. Two Cu(II) atoms are bridged by one $\mathbf{L_1}$ ligand to form a zigzag chain with the Cu···Cu distance of 10.257(1) Å (Fig. 2b). Additionally, in the molecular packing, there exists a type of hydrogen bond (C–H···Cl) (C7–H7A···Cl3, 3.4919 Å, 139.19°; C11–H11A···Cl3, 3.478 Å, 152.20°), which further enhances the stability of the molecular structure.

*3.2.2.2. $[Cu_{0.5}(\mathbf{L_2})_{0.5}Cl]_n$ (**2**).* The asymmetric unit of complex **2** is made up of a half copper atom, a half of $\mathbf{L_2}$ ligand and one chlorine atom (Fig. 3a). Each Cu(II) atom coordinates to two nitrogen atoms from two $\mathbf{L_2}$ ligands and two chlorine atoms to form a parallelogram geometry coordination environment. The center metal coordination environment of the complex **2** is similar to that of **1**. The bond distances of Cu–N_{pz} and Cu–Cl are 1.977(2) and 2.2511(8) Å, respectively. The N–Cu–N bond angle is 180.0° and the angles of N–Cu–Cl are in the range of 87.36(6)–90.63(6)°. The dihedral angle of between benzene ring and pyrazole ring is 72.8(2)°. Adjacent copper centers are separated by $\mathbf{L_2}$ ligand with a distance of 8.840(4) Å and extend along an axis to form a makro-radian helical chain (Fig. 3b). The adjacent chains are further linked by intermolecular weak interactions between carbon atom from benzene ring and the coordinated chlorine atom (C9–H9···Cl1$^{\#3}$, 3.6360 Å, 170.83°, #3: x, 1+y, z) to afford a 2D supermolecular network structure along ab plane (Fig. 3c).

*3.2.2.3. $[Ag_{0.5}(\mathbf{L_2})_{0.5}(NO_3)]_n$ (**3**).* The composition of the complex **3** is similar to that of the complex **2** except that starting material of $CuCl_2{\cdot}2H_2O$ was replaced by $AgNO_3$. The Ag(I) atom adopts a distorted tetrahedron geometry with two nitrogen atoms from two $\mathbf{L_2}$ ligands and two oxygen atoms from a nitrate group (Fig. 4a). The lengths of Ag–N and Ag–O are 2.210(8) and 2.585(11) Å,

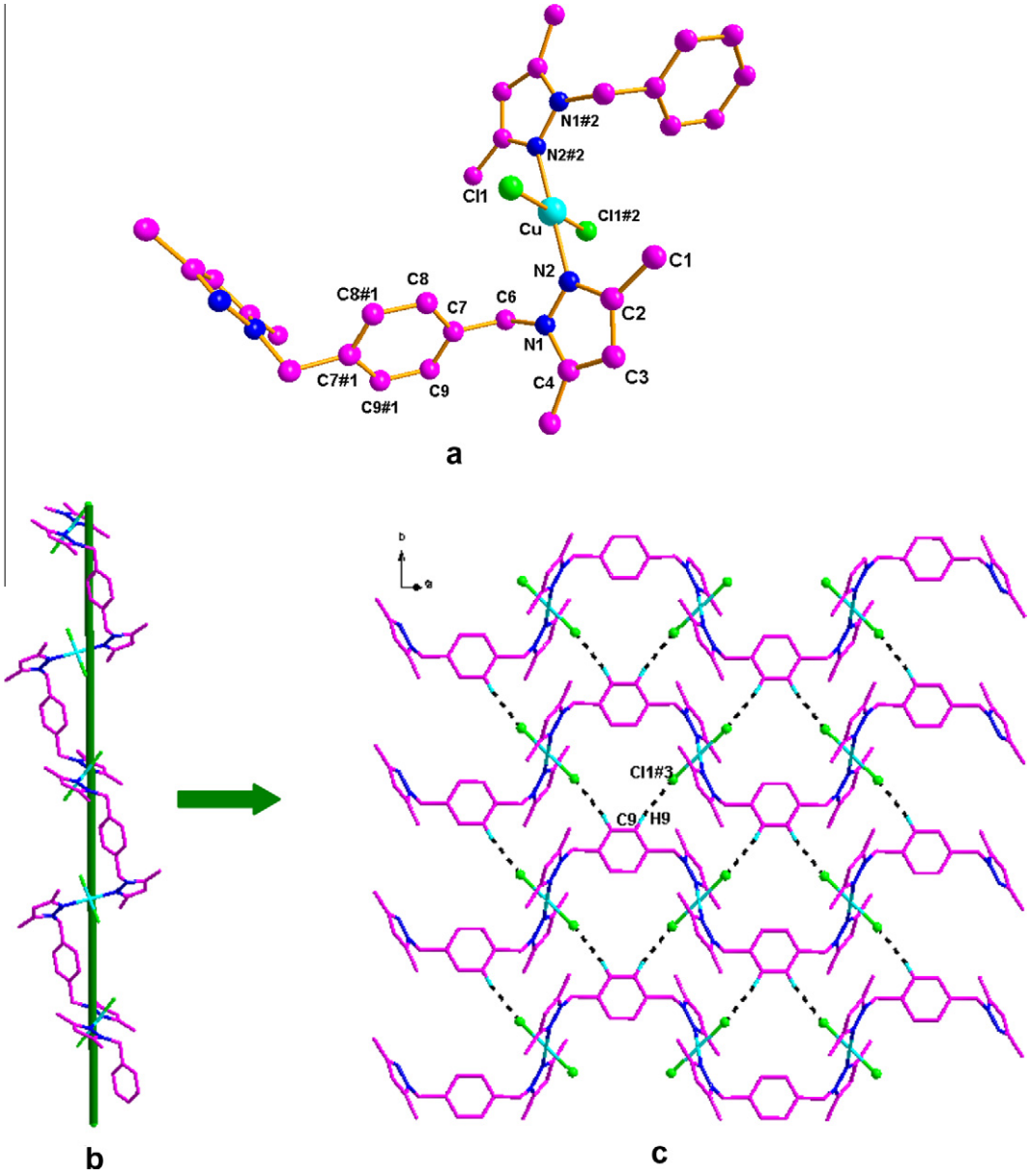

Fig. 3. (a) Local coordination environment of Cu(II) atom in **2**; (b) A view of an infinite helical chain along the [0 1 0] direction in the complex **2** (the hydrogen atoms are omitted for clarity); (c) A view of sheet structure formed by the hydrogen bonds linked helical chains in the ab plane.(a part of hydrogen atoms are omitted for clarity) (#1: −x, y, 0.5−z; #2: 0.5−x, 0.5−y, 1−z; #3: x, 1+y, z).

respectively. The axial bond angle of N–Ag–N is 129.9(4)° and the bond angles of N–Ag–O are in the range of 108.8(4)–116.9(4)°. The adjacent Ag atoms are linked through $\mathbf{L_2}$ ligand to form a 1D Ag–$\mathbf{L_2}$–Ag polymeric chain along [0 1 0] direction (Fig. 4b). These parallel chains are further connected by the hydrogen bond of C6–H6B···O2 [C6–H6B···O2$^{\#3}$, 3.3672 Å, 152.70°, #3: 1−x, −y, −z; C6$^{\#4}$–H6B$^{\#4}$···O2$^{\#3}$, 3.3672 Å, 152.70°, #4: 1−x, y, −1/2−z] to give a layer in the ac plane (Fig. 4c). When viewed along the [1 0 0] direction, the NO_3^- further linked these layers to construct a 3D supermolecular network (Fig. 4d).

*3.2.2.4. [Zn($\mathbf{L_2}$)(SCN)$_2$]$_n$ (**4**).* The Zn(II) atom adopts a distorted tetrahedral geometry with four nitrogen atoms (N1, N2, N4, N5) from pyrazolyl rings of two $\mathbf{L_2}$ ligands and two thiocyanate groups, respectively (Fig. 5a). The bond lengths of Zn(II)–N_{pz} and Zn(II)–N_{SCN} are 2.019(9)/2.053(9) and 1.934(10)/1.964(11) Å, respectively. Analysis of molecular conformation reveals two [Zn(SCN)$_2$] units are linked by one $\mathbf{L_2}$ ligand in a trans-conformation to afford a binuclear unit featuring a 16-membered ring with the average of the Zn···Zn distance of 8.65 Å. The dihedral angles between pyrazolyl ring and phenyl ring are 86.3(9) and 86.9(9)°, respectively. The dihedral angle between two pyrazolyl rings is 80.9(5)°. The polymer chain propagates via b-glide (Fig. 5b), and by the C–H···S hydrogen bond (C5–H5A···S2$^{\#3}$, #3: −x, 1−y, 1−z, 3.7670 Å, 155.05°; C11–H11···S2$^{\#4}$, 3.6100 Å, 139.67°, #4: 1+x, y, z), further to form an intercross-hydrogen bonding network (Fig. 5c).

*3.2.2.5. [Cd($\mathbf{L_2}$)$_{0.5}$(SCN)$_2$]$_n$ (**5**).* The asymmetric unit of **5** contains one Cd(II) atom, a half $\mathbf{L_2}$ ligand and two thiocyanate ions, described as a distorted trigonal bipyramidal geometry (Fig. 6a). The Cd center is surrounded by two N atoms and two S atoms from four NCS groups, and one N atom from $\mathbf{L_2}$ ligand (Cd–N: 2.270(4)–2.297(3) Å; Cd–S: 2.609(1), 2.735(1) Å)). Each two NCS groups bind to two adjacent Cd^{2+} by the bridging bidentate coordination mode to form a helix-chain with the Cd···Cd distance of 5.772(2) and 5.738(2) Å, respectively (Fig. 6b). The helix-chain is further

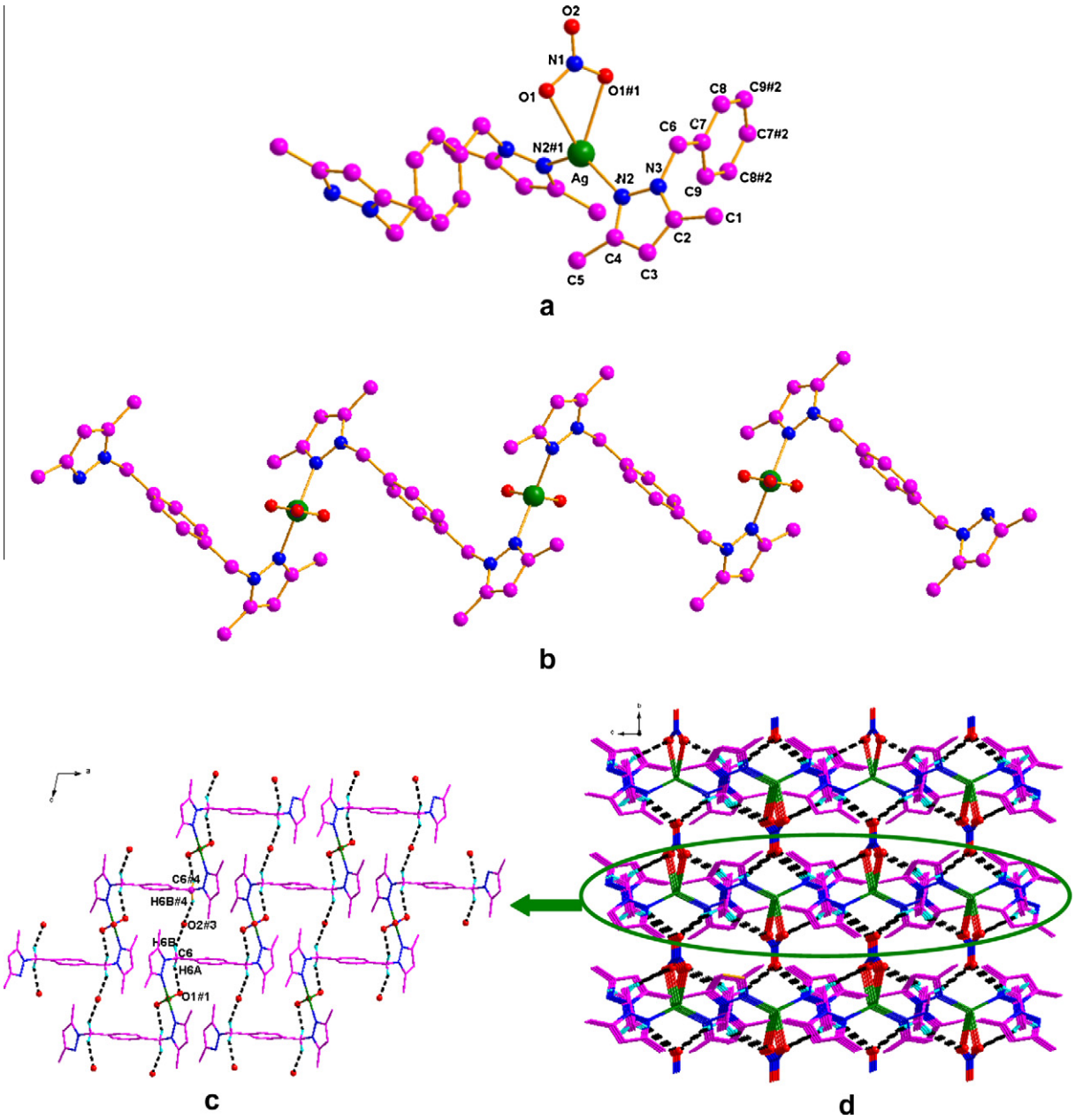

Fig. 4. (a) Local coordination environment of the Ag(I) atom in **3**; (b) a wavelike chain viewed along [0 1 0] direction in the complex **3**. (the hydrogen atoms are omitted for clarity); (c) sheet structure formed by hydrogen bond of C6–H6B···O2 linked parallel chains in the ac plane; (d) The 3D packing framework of the complex **3**. (a part of hydrogen atoms are omitted for clarity)(#1: −x+1, y, −z+1/2; #2: 3/2−x, 1/2−y, z; #3: 1−x, −y, −z; #4: 1−x, y, −1/2−z).

bridge-linked by $\mathbf{L_2}$ ligand to generate a laminated polymer (Fig. 6c).

3.3. IR spectra

The IR spectra of the ligands $\mathbf{L_1}$–$\mathbf{L_6}$ (Fig. S1–6) exhibit weak absorption bands in the range of 3139–3030 cm^{-1} and strong absorption bands in the range of 824–797 cm^{-1}, indicating the presence of the C–H(=C–H) stretching vibrations and bending vibrations, respectively. Absorption bands at 2995–2851 cm^{-1} should be assigned to the stretching vibrations of the C–H (–CH_3, –CH_2). The bands in the region of 1638–999 cm^{-1} are attributed to the aromatic skeleton stretching vibration of the pyrazolyl and benzene rings. As for $\mathbf{L_3}$ and $\mathbf{L_4}$, the bands at 608 and 595 cm^{-1} are characteristic of C–I. As for $\mathbf{L_5}$ and $\mathbf{L_6}$, the peaks at 1530, 1561, 1328 and 1356 cm^{-1} are due to asymmetry and symmetry stretching vibrations of nitro-group, respectively. In addition, the detailed appointment of the IR spectra data for ligands $\mathbf{L_1}$–$\mathbf{L_6}$ is shown in Table S1. Comparison of IR characterization for $\mathbf{L_1}$–$\mathbf{L_6}$ found that the stretching vibration frequency of "=C–H" for pyrazolyl moiety are slightly larger than those of 3,5-di-methyl-pyrazolyl moiety, and the stretching vibration of =C–H for $\mathbf{L_1}$, $\mathbf{L_5}$ splits into two peaks (3116 and 3090 cm^{-1} for $\mathbf{L_1}$, 3119 and 3139 cm^{-1} for $\mathbf{L_5}$).

The IR spectra data of the complexes **1**–**5** (Fig. S7–11) was listed in Table S2. It is clearly found that stretching vibrations of C–H(=C–H, –CH_3, –CH_2) is in the range of 3132–3030 cm^{-1}. The strong peaks in the range of 1636–1022 cm^{-1} account for the appearance of C=C, C=N of the pyrazole and benzene rings, which generate slightly blue shift through comparison of that of corresponding to the ligands. For complex **3**, the characteristic bands of NO_3^- anion are shown at 1552 cm^{-1} for asymmetric stretching vibrations and 1384 cm^{-1} for symmetric stretching vibrations,

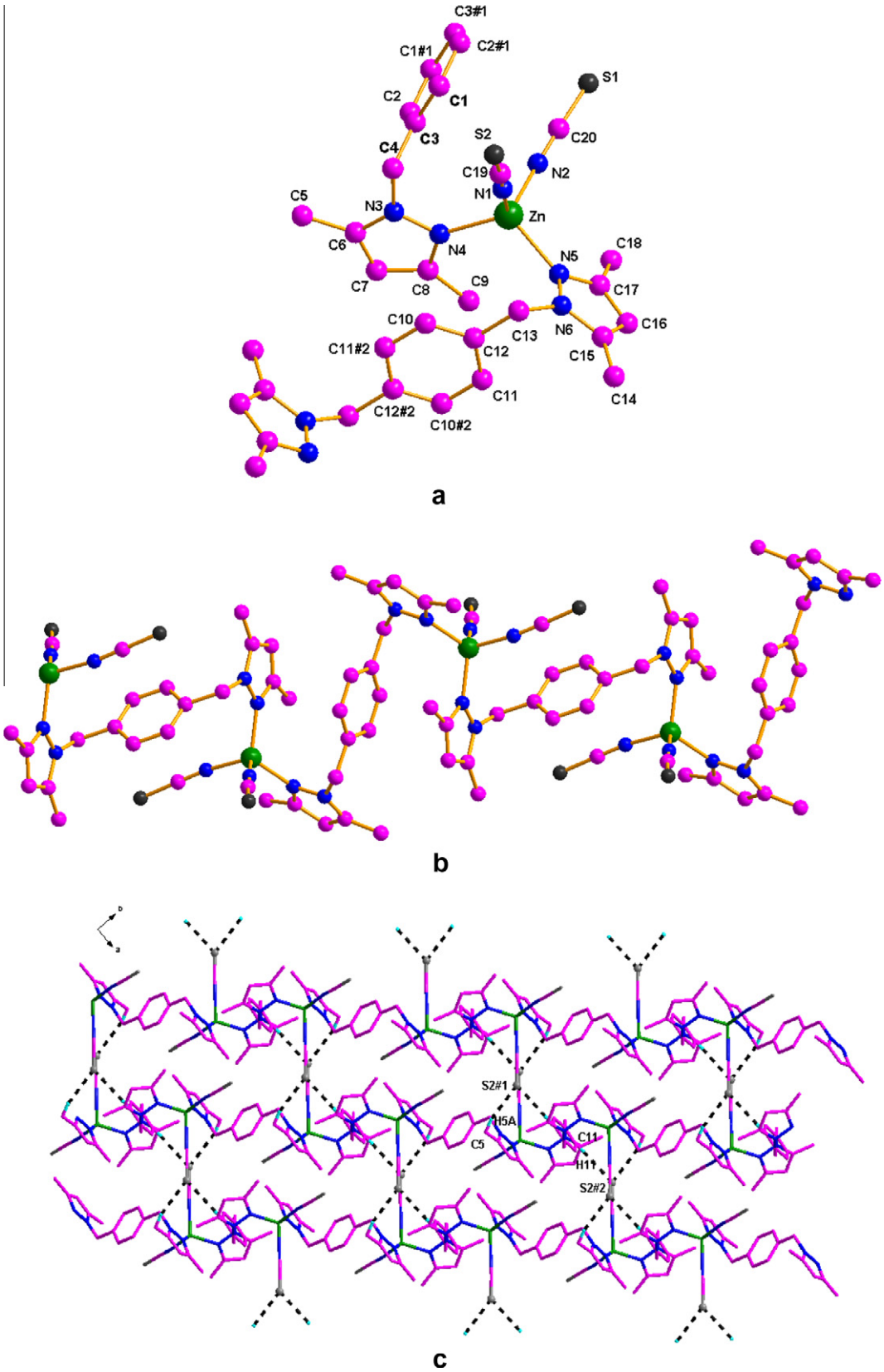

Fig. 5. (a) Local coordination environment of the Zn(II) atom in **4**; (b) 1D Zn–$\mathbf{L_2}$–Zn polymeric chain of the complex **4** along [0 1 0] direction; (c) a intercross-hydrogen bonding network formed by the hydrogen bonds(C–H···S) in the ab plane. (a part of hydrogen atoms are omitted for clarity)(#1: −x, −y, 1−z; #2: 1−x, 1−y, 1−z; #3: −x, 1−y, 1−z; #4: 1+x, y, z).

which is agreement with those of the related Ag complexes [35]. There are sharp and strong absorption bands in the region of 2083–2125 cm^{-1} for **4** and **5**, which is assigned to the asymmetric stretching frequency of the thiocyanate groups. While stretching

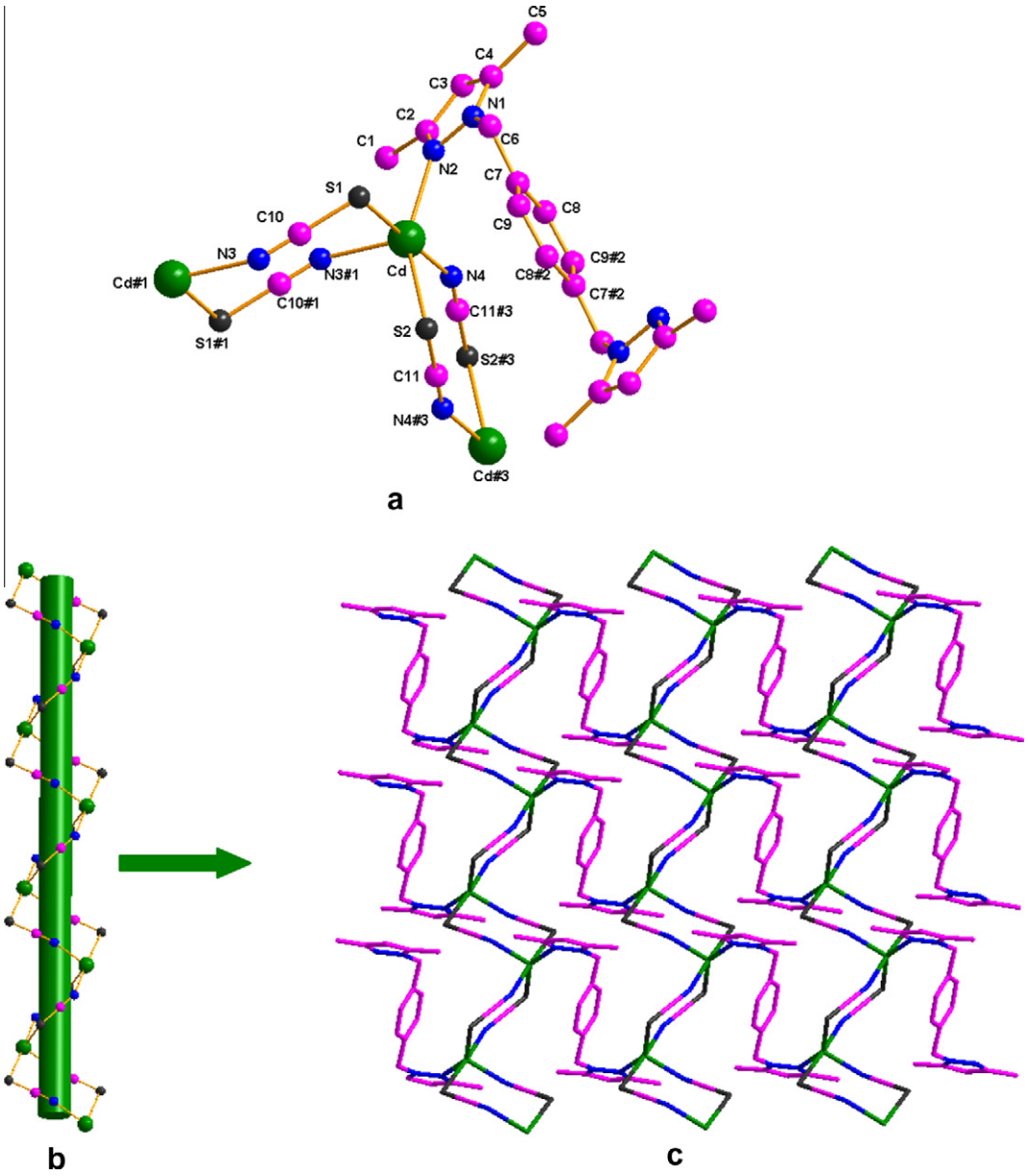

Fig. 6. (a) Local coordination environment of the Cd(II) atom in **5**; (b) helical chain is formed through the two thiocyanate bridging the Cd(II) atoms along [001] direction in complex **5** (a part of hydrogen atoms and SNC groups are omitted for clarity); (c) ladder-like tapes layer in the ab plane. (a part of hydrogen atoms are omitted for clarity)(#1: −x+2, −y, −z+1; #2: −x+2, −y+1, −z; #3: −x+2, −y, −z).

vibration of thiocyanate group for complex **5** splits into two strong peaks, this is because there are two types of coordination environment of the thiocyanate group.

Additionally, the compositions of complexes **1**–**5** were confirmed by elemental analysis and X-ray powder diffraction (PXRD) was used to confirm the phase purity of the bulk materials (Fig. S12–16). The experiment results prove that all the peaks presented in the measured patterns closely match the simulated patterns generated from single crystal diffraction data.

3.4. ^1H NMR spectra

The structures of these compounds (**L_1**–**L_6**) were further confirmed by ^1H and ^{13}C HMR spectra through comparison with the spectra of the related compounds [36]. ^1H and ^{13}C NMR spectra of ligands **L_1**–**L_6** (Table S3 and S4, Fig. S18–29) were recorded in $CDCl_3$ or DMSO-d_6. According to chemical shift of proton, it is found that the proton resonances of pyrazolyl ring of nitro substituted compounds (**L_5** and **L_6**) move obviously to downfield, the signals of H^4-pz of **L_2** move to upfield (5.82 ppm for **L_2**; 6.26 ppm for **L_1**). Similarly, the signals in ^{13}C NMR spectra of ligands **L_1**–**L_6** are divided into three groups according to the different substituted group on C4: (i) 106.02 ppm for **L_1** and 105.53 ppm for **L_2**, are assigned to no substituted group on C4; (ii) the chemical shift of 4-iodo-substituted compounds (56.62 ppm for **L_3** and 63.27 ppm for **L_4**) in upfield; (iii) the signals of 4-nitro-substituted compounds (135.04 ppm for **L_5** and 131.60 ppm for **L_6**) in downfield. ^1H and ^{13}C NMR spectra of complexes **1**–**5** (Table S5 and S6, Fig. S30–39) were recorded in $CDCl_3$ or DMSO-d_6. The chemical shift of ^1H NMR spectra of the complex **1** and **2** due to ligands being coordinated to copper atom to turn in considerably broad, which seems to indicate that the copper complexes are paramagnetic. Compared with chemical shift of the corresponding ligands, the chemical shift

of H^4-pz of complexes**1**–**3** move to downfield, however, that of complexes **4** and **5** containing SCN groups went on upfield. The ^{13}C NMR spectra of all complexes are very similar and it is almost not any influence on the compounds and the complexes.

3.5. UV–Vis absorption spectra

The electronic absorption spectra of the complexes **1**–**5** are recorded. As shown in Fig. S40. Bands at 208 nm for **1**, 206 nm for **2**, 206 nm for **3**, 208 nm for **4** and 212 nm for **5** are attributed to the π–π* transition of the ligands. Compared with the π–π* transition of the ligand $\mathbf{L_2}$ (214 nm), it is found that the characterization absorption bands of the complexes **2**–**5** move slightly to blue-shift. The band at 404 nm for **1** and 422 nm for **2** are assigned to the charge transitions from the ligands to Cu(II) atom (LMCT) of N → Cu. The broad peak at 780 nm for **1** and 610 nm for **2** can be caused by the d → d* transition of Cu^{2+} cation, respectively [37].

3.6. Luminescent properties

The fluorescence of inorganic-organic coordination polymers especially those with the d^{10} metal center [38,39], is drawing significant attention for their potential applications as fluorescent-emitting materials, such as light-emitting diodes (LEDs) [40–42]. Hereupon, it is necessary to investigate the photoluminescent property with the d^{10} metal coordination polymers. In general, as for the d^{10} metal centers of the Ag(I), Zn(II) or Cd(II), the emission band of these complexes may be assigned to the LLCT, incorporation with MLCT and LMCT [43–45]. The photoluminescence properties of complexes **3**–**5** and ligand ($\mathbf{L_2}$) were studied in the solid state at room temperature (Fig. 7). It is found that emission bands are observed at 301 and 417 nm ((λ_{ex} = 260 nm) for $\mathbf{L_2}$, which can be ascribed to the π* → n or π* → π transitions of the organic ligand. An intense emission peak (432 nm) of complex **4** at the excitation wavelength of 378 nm with slit width (3:1) is observed, and a phenomena of red shift 15 nm occurred as compared with that of the $\mathbf{L_2}$ ligand (λ_{em} = 417 nm). Strong emission bands in the range of 370–385 nm (λ_{ex} = 341 nm) and 368–383 nm (λ_{ex} = 324 nm) are exhibited for the complexes **3** and **5**, which occurred a blue-shifted as compared with the $\mathbf{L_2}$ ligand (λ_{em} = 417 nm), respectively. The results above match with the absorption spectra of the complexes. The enhancement of luminescence in complexes **3**–**5** compared with free ligand $\mathbf{L_2}$ may be attributed to the enhancement of the rigidity of the ligand and the reduction of the loss of energy through a radiationless pathway [46], while, the emission of complexes **3**–**5** occurs red-shifted or blue-shifted, which is probably due to the different coordination modes and the metal centre with the same ligand.

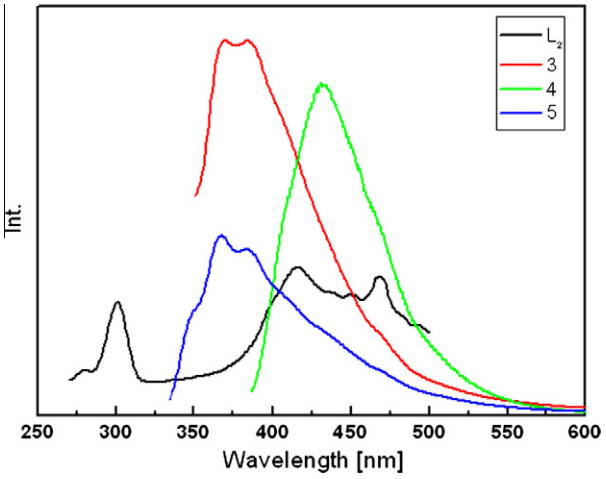

Fig. 7. Solid-state emission spectra of complexes **1**–**5** and the ligand $\mathbf{L_2}$ at room temperature.

3.7. Thermal properties

To examine the thermal stability of the coordination polymers, thermogravimetric analyses (TGA) were carried out under N2 atmosphere of the complexes 1–5 (Fig. 8) in the temperature range of 25–1000 °C. The TGA curve of **1** shows that the weight loss of 63.34% between 152 and 714 °C is attributed to the release of the organic ligand (Calc. 64.10%), the residue is copper chloride (obsd: 34.41%; Calc.: 36.07%). The first weight loss in the complex **2** occurs in the range 217–335 °C, implying the removal of the 3,5-dimethyl-1*H*-pyrazole and methylene (obsd: 48.06%, Calc.: 47.17%). The second weight loss of 16.83% occurs in the temperature range of 350–442 °C, which is ascribed to the release of the benzene ring (Calc. 17.76%). Finally, the residue is corresponding copper nitride (obsd: 14.35%; Calc.: 17.00%). In the complex **3**, the result shows a first major weight loss equal to 64.20% in the range 206–299 °C, ascribed to the release of organic ligands (Calc. 63.41%). So, the framework is stable up to 206 °C, at which point the removal of nitrate radical can ensue. The residue is corresponding to silver oxide (obsd: 25.31%; Calc.: 24.96%). Complex **4**–**5** can keep the stability before 202 °C, and then the pyrazolyl ring, methylene, benzene ring and thiocyanate collapse slowly in turn. The decomposition of the remaining substance finished at 860 °C. Finally, the residue corresponds to zinc nitride and cad-

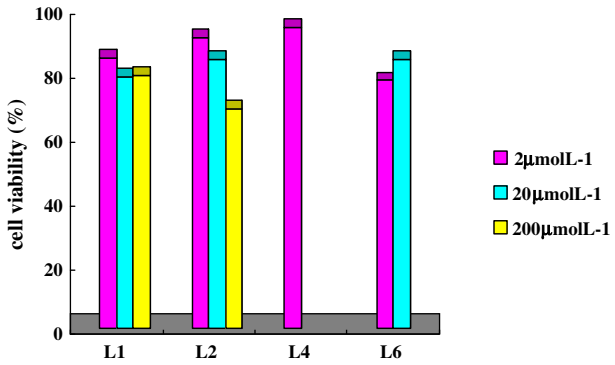

Fig. 8. Effect of the different concentration of the compounds $\mathbf{L_1}$–$\mathbf{L_6}$ on the viability of hepG2 cell.

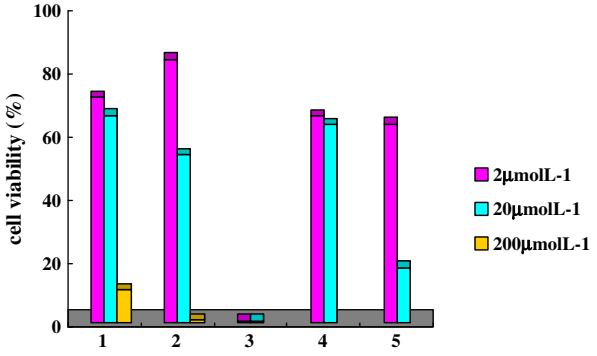

Fig. 9. Effect of the concentration of complexes **1**–**5** on the viability of hepG2 cell.

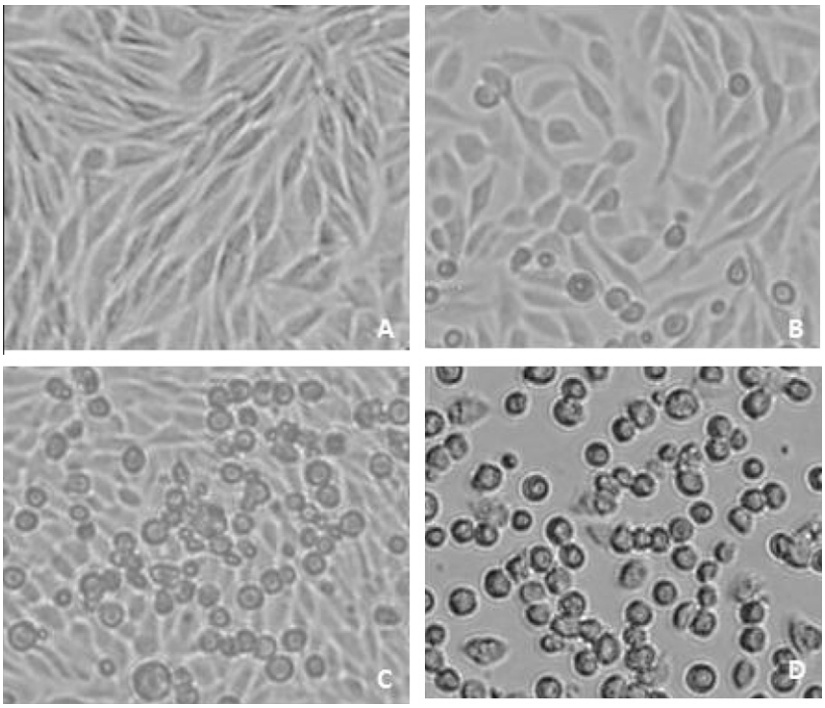

Fig. 10. HepG-2 cells were incubated with various concentrations of complex **2** for 24 h. (A) normal cell (B) 2 μmol/L (C) 20 μmol/L (D) 200 μmol/L.

mium nitride (obsd: 15.31%, 31.49% for **4**; Calc.: 13.74%, 29.91% for **5**).

3.8. Statistical analysis

Results are expressed as x ± s. Statistical differences were determined between groups by one-way analysis of variance (ANOVA) and Tukey's multiple comparison test. Statistically significant differences between groups were defined as $P < 0.05$. Calculations were performed with the Graph Pad and Prism program (Table S7).

3.9. Biological assays

The cytotoxicity of synthesized compounds $\mathbf{L_1}$–$\mathbf{L_6}$ and complexes **1**–**5** were evaluated using a 24 h continuous exposure against hepG2 cells in vitro at several concentrations (Figs. 7 and 8). The results showed that most compounds can suppress hepG2 cell growth. It presents the differences for a variety of compounds according to some extent of the restriction on the growth of hepG2 cells. The rate of inhibition enhances with the concentration of compound increasing. Among ligands, $\mathbf{L_3}$ and $\mathbf{L_5}$ precipitate at only 2 μmol L^{-1}. $\mathbf{L_2}$ causes 9, 16 and 28% of cell death at 2, 20 and 200 μmol L^{-1}, respectively. Similar behavior was observed for other ligands. The Research found that the substitute of the pyrazolyl ring strongly influenced the cytotoxicity of the compounds. The nitro-substituted compounds are higher inhibiting than the other group substituted compounds at 2 μmol L^{-1}. For complexes **1**–**5**, the complexes provoke cell death obviously increased than the corresponding ligands. Therefore, the particular role of metals in cytotoxicity may be as an important inhibitory reagent. In addition, it can be seen that different metals have different influence on hepG2 cell growth when the ligand in the complexes is the same, especially, at 2 μmol L^{-1}, there are 99% cell death in the complex **3**, because silver ion is more powerful to strengthen the cell membrane damage.

The effects of the various concentrations of the compound induced apoptosis in hepG-2 cells. For instance, hepG2 cells were incubated with various concentrations of complex **2** for 24 h (Fig. 9). This figure shows the complex **2** treated cells narrowed to go round and chromatin condensed, suggesting they are undergoing apoptosis (see Fig. 10).

4. Conclusion

In conclusion, a new series of M–$\mathbf{L_2}$–M coordination polymers were synthesized and characterized for the first time. X-ray diffraction results that the layer structure and 3D microporous framework of all the complexes were constructed by the different ligands and metal atoms. Although the ligand displays the same conformation and coordination mode, introducing of the small molecular organic reagent leads to form various coordination modes and play a key role in the construction of the high dimensional architecture. Simultaneously, the photoluminescence behaviours analysis of the different structures are theoretically significant for understanding of the relationship between the structures and photoluminescence properties of the complexes. The study results show that the complexes **3**–**5** seem to be good candidates for novel hybrid inorganic–organic photoactive materials. Furthermore, the cytotoxicity of the ligands and complexes **1**–**5** was evaluated against hepG2 cells. The results showed that the complexes **1**–**5** provoke cell death obviously increased than the corresponding ligands. Finally, these interesting materials hint us to further research the rational synthetic strategy for obtaining new complexes with potential bioactivity properties and multiple structures.

Acknowledgements

This work was supported by the grants of the National Natural Science Foundation of China (Grant No. 21071071) and State Key Laboratory of Inorganic Synthesis and Preparative Chemistry, Col-

lege of Chemistry, Jilin University, Changchun 130012, PR China (Grant No. 2013-05).

Appendix A. Supplementary data

CCDC 833039(**L3**), 833043(**L4**), 833044(**L5**), 833048(**1**), 833049(**2**), 833041(**3**), 833050(**4**) and 833040(**5**); contains the supplementary crystallographic data for **L3**–**L5** and complexes **1**–**5**. These data can be obtained free of charge via http://www.ccdc.cam.ac.uk/conts/retrieving.html, or from the Cambridge Crystallographic Data Centre, 12 Union Road, Cambridge CB2 1EZ, UK; fax: (+44) 1223 336 033; or e-mail: deposit@ccdc.cam.ac.uk. Supplementary data associated with this article can be found, in the online version, at http://dx.doi.org/10.1016/j.poly.2012.08.016.

References

[1] X.Y. Jin, W.J. Yang, Z.S. Qian, Y.J. Wang, S.P. Bi, J.C.S. Dalton Trans. 40 (2011) 5052.
[2] H.P. Zhou, X.P. Gan, X.L. Li, Z.D. Liu, W.Q. Geng, F.X. Zhou, W.Z. Ke, P. Wang, L. Kong, F.Y. Hao, J.Y. Wu, Y.P. Tian, Cryst. Growth Des. 10 (2010) 1767.
[3] F. Silva, F. Marques, I.C. Santos, A. Paulo, A.S. Rodrigues, J. Rueff, I. Santos, J. Inorg. Biochem. 104 (2010) 523.
[4] M.X. Li, L.Z. Zhang, C.L. Chen, J.Y. Niu, B.S. Ji, J. Inorg. Biochem. 106 (2012) 117.
[5] D.L. Reger, E.A. Foley, R.P. Watson, P.J. Pellechia, M.D. Smith, Inorg. Chem. 48 (2009) 10658.
[6] S. Trofimenko, Scorpionates II: Chelating Borate Ligands, Imperial College Press, London, 2008.
[7] C. Pettinari, Scorpionates II: Chelating Borate Ligands, World Scientific Publishing Co., Singapore, 2008.
[8] Y.J. Sun, L.Z. Zhang, P. Cheng, H.K. Lin, S.P. Yan, W. Sun, D.Z. Liao, Z.H. Jiang, P.W. Shen, Inorg. Chem. 42 (2003) 508.
[9] L.L. Blosch, K. Abboud, J.M. Boncella, J. Am. Chem. Soc. 113 (1991) 7066.
[10] A.S. Potapov, E.A. Nudnova, G.A. Domina, L.N. Kirpotina, M.T. Quinn, A.I. Khlebnikov, I.A. Schepetkin, J.C.S. Dalton Trans. (2009) 4488.
[11] D.L. Reger, R.P. Watson, M.D. Smith, J. Organomet. Chem. 692 (2007) 5414.
[12] C. Pettinari, R. Pettinari, Coord. Chem. Rev. 249 (2005) 525.
[13] P. Govindaswamy, P.J. Carroll, Y.A. Mozharivskyj, K.M. Rao, J. Organomet. Chem. 690 (2005) 885.
[14] G. Gupta, K.T. Prasad, B. Das, G.P.A. Yap, K.M. Rao, J. Organomet. Chem. 694 (2009) 2618.
[15] D.L. Reger, R.P. Watson, M.D. Smith, P.J. Pellechia, Organometallics 24 (2005) 1544.
[16] D.L. Reger, R.P. Watson, J.R. Gardinier, M.D. Smith, P.J. Pellechia, Inorg. Chem. 45 (2006) 10088.
[17] C.M. Hartshorn, P.J. Steel, Inorg. Chem. Commun. 3 (2000) 476.
[18] I. Stein, U. Ruschewitz, Z. Anorg, Allg. Chem. 635 (2009) 914.
[19] Y.H. Xing, Y.H. Zhang, Z. Sun, L. Ye, Y.T. Xu, M.F. Ge, B.L. Zhang, S.Y. Niu, J. Inorg. Biochem. 101 (2007) 36.
[20] J.X. Chen, D.M.L. Goodgame, S. Menzer, D.J. Williams, Polyhedron 16 (1997) 1679.
[21] G.F. Hou, L.H. Bi, B. Li, L.X. Wu, Inorg. Chem. 49 (2010) 6474.
[22] S. Scheuermann, T. Kretz, H. Vitze, J.W. Bats, M. Bolte, H.W. Lerner, M. Wagner, Chem. Eur. J. 14 (2008) 2590.
[23] S. Wang, H.Y. Zang, C.Y. Sun, G.J. Xu, X.L. Wang, K.Z. Shao, Y.Q. Lan, Z.M. Su, Cryst. Growth Des. 12 (2010) 3458.
[24] G. Margraf, T. Kretz, F. Fabrizi de Biani, F. Laschi, S. Losi, P. Zanello, J.W. Bats, B. Wolf, K.R. Langer, M. Lang, A. Prokofiev, W. Assmus, H.W. Lerner, M. Wagner, Inorg. Chem. 45 (2006) 1277.
[25] C.M. Hartshorn, P.J. Steel, Aust. J. Chem. 48 (1995) 1587.
[26] E.A. Nudnova, A.S. Potapov, A.I. Khlebnikov, V.D. Ogorodnikov, Russ. J. Org. Chem. 43 (2007) 1698.
[27] Submitted by J.M. Snell and A. Weissberger. Checked by R. L. Shriner and N.S. Moon. Organic Syntheses, Coll. vol. 3, 1955, p. 788; vol. 20, 1940, p. 92.
[28] M.M. Kim, R.T. Ruck, D. Zhao, M.A. Huffman, Tetrahedron Lett. 49 (2008) 4026.
[29] C.L. Habraken, J.W.A.M. Janssen, J. Org. Chem. 36 (1971) 3081.
[30] Q. Jin, J.X. Nan, L.H. Lian, Chin. J. Nat. Med. 9 (2011) 61.
[31] G.M Sheldrick, SADABS, Program for Empirical Absorption Correction for Area Detector Data; University of. Göttingen, Göttingen, Germany, 1996 and 2003.
[32] G.M. Sheldrick, SHELX-97, Program for Crystal Structure Refinement, University of Göttingen, Göttingen, Germany, 1997.
[33] D.L. Reger, R.P. Watson, J.R. Gardinier, M.D. Smith, Inorg. Chem. 43 (2004) 6609.
[34] J.L. Bongiovanni, B.W. Rowe, P.T. Fadden, M.T. Taylor, K.R. Wells, M. Kumar, E.T. Papish, G.P.A. Yap, M. Zeller, Inorg. Chim. Acta 363 (2010) 2163.
[35] N.F. Curtis, Y.M. Curtis, Inorg. Chem. 4 (1965) 804.
[36] C.H. Hartshorn, P.J. Steel, Aust. J. Chem. 48 (1995) 1587.
[37] K. Fujisawa, H. Iwamoto, K. Tobita, Y. Miyashita, K. Okamoto, Inorg. Chim. Acta 362 (2009) 4500.
[38] S.L. Zheng, J.H. Yang, X.L. Yu, X.M. Chen, W.T. Wong, Inorg. Chem. 43 (2004) 830.
[39] B. Ding, L. Yi, Y. Wang, P. Cheng, D.Z. Liao, S.P. Yan, Z.H. Jiang, H.B. Song, H.G. Wang, J.C.S. Dalton Trans. (2006) 665.
[40] T.L. Hu, R.Q. Zou, J.R. Li, X.H. Bu, J.C.S. Dalton Trans. (2008) 1302.
[41] W. Chen, J.Y. Wang, C. Chen, Q. Yue, H.M. Yuan, J.S. Chen, S.N. Wang, Inorg. Chem. 42 (2003) 944.
[42] P. Cui, Z. Chen, D.L. Gao, B. Zhao, W. Shi, P. Cheng, Cryst. Growth Des. 10 (2010) 4370.
[43] Q. Shi, Y.T. Sun, L.Z. Sheng, K.F. Ma, M.L. Hu, X.G. Hu, S.M. Huang, Cryst. Growth Des. 8 (2008) 3401.
[44] X.F. Li, T.F. Liu, B. Hu, G.L. Li, H. Zhang, R. Cao, Cryst. Growth Des. 10 (2010) 3051.
[45] X.L. Wang, C. Qin, E.B. Wang, Y.G. Li, N. Hao, C.W. Hu, L. Xu, Inorg. Chem. 43 (2004) 1850.
[46] Y. Liu, P.F. Yan, Y.H. Yu, G.F. Hou, J.S. Gao, Y. Lu, Cryst. Growth Des. 10 (2010) 1559.